

Optical properties of recent non-fullerene molecular acceptors for bulk heterojunction solar cells

Andrea Farina¹, Giuseppe M. Paternò², Francesco Scotognella^{2,3*}

¹ *Istituto di Fotonica e Nanotecnologie, Consiglio Nazionale delle Ricerche, Piazza Leonardo da Vinci 32, 20133 Milano, Italy*

² *Center for Nano Science and Technology@PoliMi, Istituto Italiano di Tecnologia, Via Pascoli 70/3, 20133 Milano, Italy*

³ *Dipartimento di Fisica, Politecnico di Milano, Piazza Leonardo da Vinci 32, 20133 Milano, Italy*

Abstract

For many years the faith of organic photovoltaics has been linked to the one of fullerene, since fullerene has been considered the electron-acceptor of choice in bulk heterojunctions solar cells. In the last years, the number of molecules that can be very competitive in replacing fullerene has increased significantly. In this work, we study by means of different theoretical methods five molecules that have demonstrated to work effectively as acceptors in organic heterojunctions. We discuss the comparison of simulated absorption spectra with the experimental spectra.

Introduction

In the last decades, fullerene-based materials have been the most used acceptors in organic bulk heterojunction solar cells, owing to their relatively high processability and to the delocalization of the lowest unoccupied molecular orbital (LUMO) across the entire three-dimensional surface of fullerene [1]. Since the first report on the use of polymer:fullerene heterojunction as photovoltaic material in 1992 [2], the use of fullerene derivatives has seen a stark increase [3–9]. On the other hand, some intrinsic limitations of fullerenes, such the generally weak optical absorption in the visible and its environmental instability [10], have promoted the research of new non-fullerene acceptors [11]. The outstanding endeavour in chasing reliable substitutes to fullerene is, for example, testified by three exhaustive review articles published in 2019 [11–13]. Remarkably, power conversion efficiencies (PCE) above 16% have been achieved for solar cells integrating the non-fullerene acceptor BTPTT-4F [14–16]. In this context, also semiconducting carbon nanotubes have been proposed as valid alternative to fullerenes, due to their excitonic behaviour and relatively high environmental stability [17–19].

In this work, we simulate by employing different calculation methods the absorption properties of non-fullerene molecules that hold great promises as efficient electron-acceptor systems in organic heterojunction solar cells. The study of the optical gap and of the different optical transitions in non-fullerene acceptors permit to corroborate and complement the experimental studies present in the literature and aims at a better understanding of the different electronic transitions in the studied molecules.

Methods

We have sketched the molecule geometries with the Avogadro package [20]. We have optimized the ground state geometries and we have calculated the electronic transitions of the molecules with the package ORCA 4.2.1 [21].

Density Functional Theory calculations (with B3LYP functional): We have used the B3LYP functional [22] in the framework of the density functional theory. We have employed the Ahlrichs split valence basis set [23] and the all-electron nonrelativistic basis set SVPalls1 [24,25]. Moreover, the calculation utilizes the Libint library [26] and the Libxc library [27,28].

Density Functional Theory calculations (with BP functional): We employ ORCA 4.2.1 [21] for these calculations. The orbital basis set def2-SVP has been used [29] and the auxiliary basis set def2/J has been used [30]. Also in this case, the calculation utilizes the Libint library [26] and the Libxc library [27,28].

Calculations with Zerner's Intermediate Neglect of Differential Overlap (ZINDO/S), Modified Neglect of Diatomic Overlap (MNDO), Parametric Method 3 (PM3) methods: Also for these calculations we employ ORCA 4.2.1 [21]. The orbital basis set def2-SVP has been used [29]. Also in this case, the calculation utilizes the Libint library [26] and the Libxc library [27,28].

Calculations with Hückel method: For the Hückel we employ the Hulis package [31,32].

Results and Discussion

In Figure 1, we show the molecular structures of the five investigated molecules. The molecule with 3-ethylrhodanine (RH) attached to both ends of thiophene-flanked carbazole is the so-called Cz-RH [33]. A solar cell that includes a bulk heterojunction with Poly(3-hexylthiophene) and Cz-RH (P3HT-Cz-RH) is reported in literature with a power conversion efficiency (PCE) of 2.56% [34].

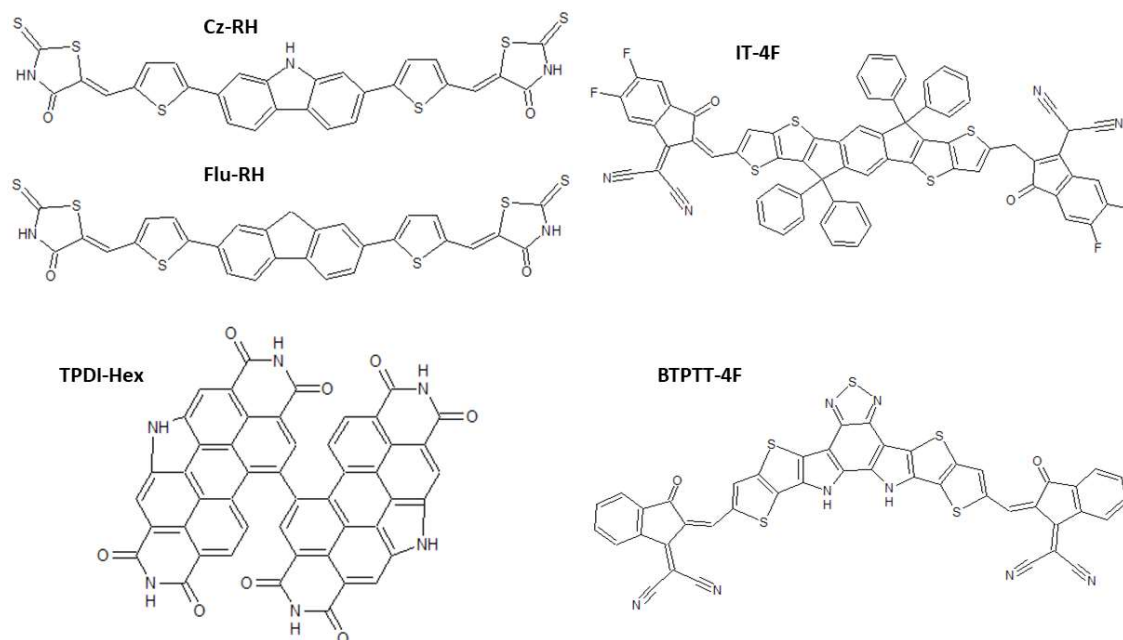


Figure 1. Molecular structures of the molecules studied: Cz-RH, Flu-RH, TPDI-Hex, IT-4F and BTPPT-4F.

The N-annulated perylene diimide (PDI) dimer has been employed in a bulk heterojunction solar cell reaching power conversion efficiency up to 7.6% with a terthiophene-based polymer named P3TEA as donor material [35]. The molecule IT-4F is used as acceptor in a bulk heterojunction with

fluorinated poly[(2,6-(4,8-bis(5-(2-ethylhexyl)thiophen-2-yl)benzo[1,2-b:4,5-b']dithiophene)-*co*-(1,3-di(5-thiophene-2-yl)-5,7-bis(2-ethylhexyl)benzo[1,2-c:4,5-c']dithiophene-4,8-dione)] (PBDB-T-SF) leads to a PCE of 13% [36,37]. Finally, a heterojunction containing BTPTT-4F shows an efficiency above 16% as mentioned above [14].

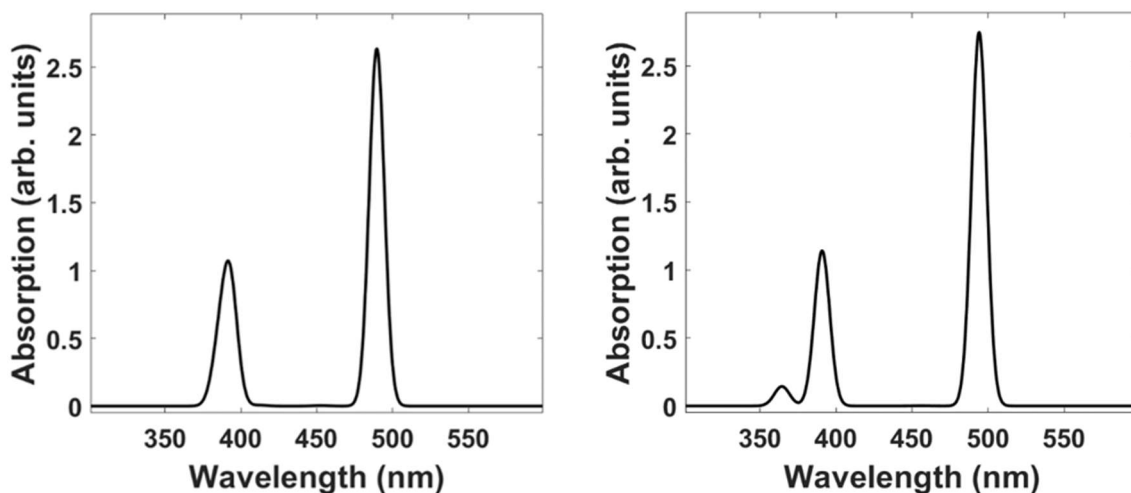


Figure 2. Calculation of the absorption spectrum (DFT with B3LYP functional) of the molecule Cz-RH (left) and the molecule Flu-RH (right).

We have calculated the first 16 transitions for the studied molecules (reported in the Supporting Information) and obtained simulated absorption spectra as a sum of Gaussian curves expressed as $f(x) = f_{osc} \exp[(x - x_c)^2 / 2a^2]$, with f_{osc} the oscillator strength of the transition, x_c the central wavelength (in nm) of the transition, a that is related to the linewidth. In particular, we have selected a value of 5 nm for the linewidth a . In Figure 2, we show the simulations of the absorption spectra of Cz-RH molecule (left) and Flu-RH molecule (right). The lowest transition peak at around 500 nm (about 2.48 eV) is in good agreement with the experimental absorption spectra for the solutions reported in Kim *et al.* [34]. The highest predicted transitions are at longer wavelengths with respect to the experimental ones.

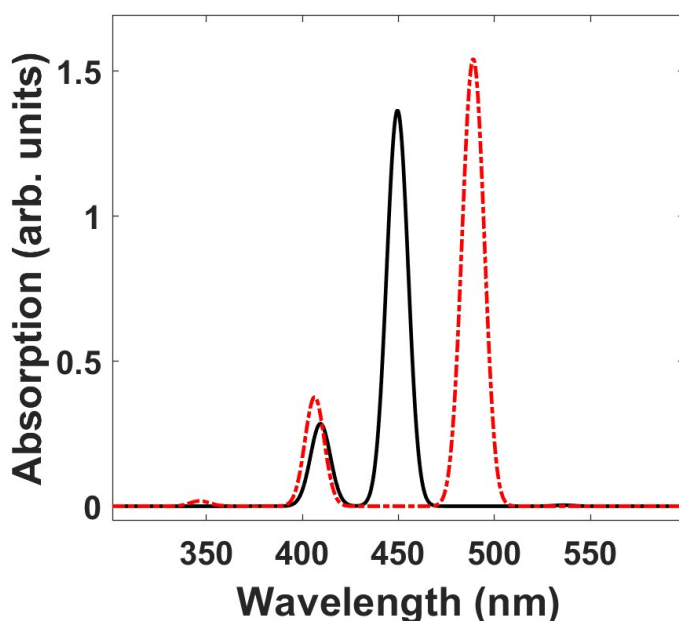


Figure 3. Calculation of the absorption spectrum of TPDI-Hex with DFT and B3LYP functional (solid black curve) and ZINDO/S method (dotted dashed red curve).

In Figure 3, we show the absorption spectrum of TPDI-Hex. We observe a discrepancy between the simulated absorption spectrum and the experimental one in terms of oscillator strength. The lowest simulated transition is at 2.31 eV (with a very weak oscillator strength of <0.01) while the lowest experimental transition is at 2.36 eV, but with a very strong weight in the spectrum with respect to the other peaks. With ZINDO/S method the simulated lowest transition is at 2.52 eV (with an oscillator strength of 0.93). These discrepancies could be due to the optimized geometry used and, in particular, to the dihedral angle between the perylene groups.

In Figure 4, we show the absorption spectrum of IT-4F with the lowest optical transition at 1.99 eV with DFT and B3LYP functional (black solid curve) and at 1.82 eV with ZINDO/S, while the experimental absorption shows the lowest absorption peak at 1.77 eV [36,37].

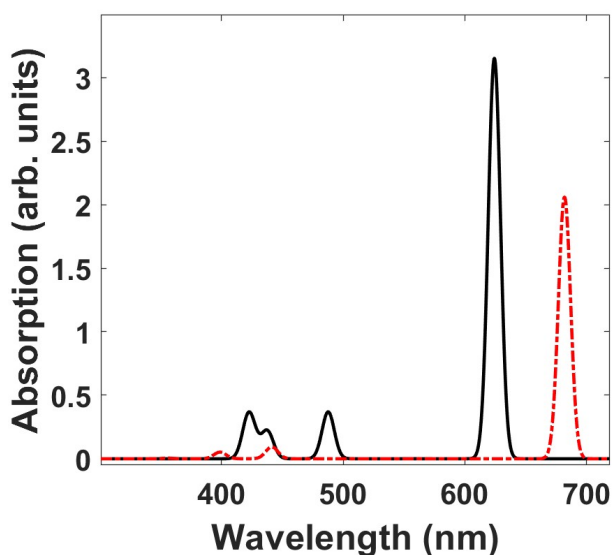


Figure 4. Calculation of the absorption spectrum of IT-4F with DFT and B3LYP functional (solid black curve) and with ZINDO/S method (dotted dashed red curve).

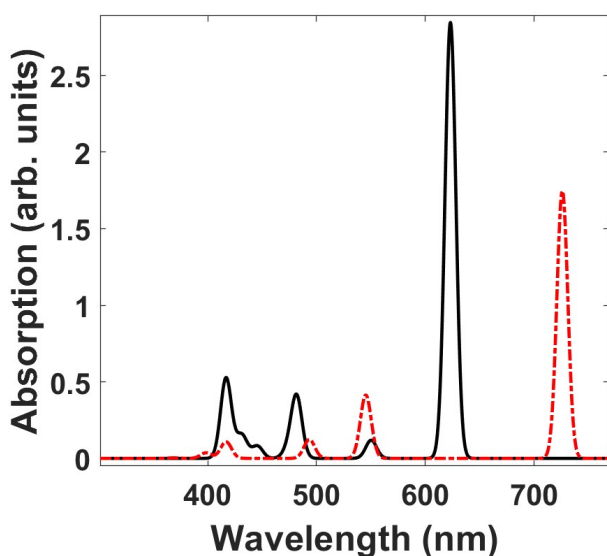


Figure 5. Calculation of the absorption spectrum of BTPTT-4F with DFT and B3LYP functional (solid black curve) and with ZINDO/S method (dotted dashed red curve).

In Figure 5, we display the absorption spectrum of BTPTT-4F, with the transition at 1.99 eV. For the estimation of BTPTT-4F optical band gap, we have employed different theoretical methods whose results are reported in Table 1.

	DFT B3LYP	DFT BP	ZINDO/S	MNDO	PM3
Optical band gap (eV)	1.99	1.65	1.71	2.01	2.28

Table 1. Optical band gap of BTPTT-4F calculated with different methods: DFT with B3LYP and BP functional, Zerner's Intermediate Neglect of Differential Overlap (ZINDO/S), Modified Neglect of Diatomic Overlap (MNDO), Parametric Method 3 (PM3).

Taking into account that Fan et al. [14] report an optical band gap of about 1.7 eV of BTPTT-4F solution

in chlorobenzene, DFT calculations with BP functional and ZINDO/S calculations give optical band gaps that are closer to the experimental one.

We perform Hückel method based calculations with Hulis package [31,32]. We find the following states: i) HOMO-1: $\alpha + 0.42\beta$; ii) HOMO: $\alpha + 0.24\beta$; iii) LUMO: $\alpha - 0.15\beta$; iv) LUMO+1: $\alpha - 0.16\beta$. Hence, we observe a HOMO-LUMO gap of 0.39β . As reported by Fan et al. [14], the experimental HOMO, measured by cyclic voltammetry, is at -5.68 eV, while the experimental LUMO is at -4.06 eV. Thus, we could estimate a value of 4.15 for the β parameter.

Conclusion

In this work, we have studied the optical properties of five different non-fullerene acceptors by means of different calculation methods. These molecules, namely Cz-RH, Flu-RH, TPDI-Hex, IT-4F and BTPTT-4F, hold great promises for application in organic photovoltaic. In regards of BTPTT-4F, which has shown remarkable photovoltaic performances in organic heterojunction cells, we have determined the optical gap and compared it with the experimental results.

Acknowledgement

G.M.P. thanks Fondazione Cariplo (grant n° 2018-0979) for financial support. This project has received funding from the European Research Council (ERC) under the European Union's Horizon 2020 research and innovation programme (grant agreement No. [816313]).

References

- [1] Y. He, Y. Li, Fullerene derivative acceptors for high performance polymer solar cells, *Phys. Chem. Chem. Phys.* 13 (2011) 1970–1983. <https://doi.org/10.1039/C0CP01178A>.
- [2] N.S. Sariciftci, L. Smilowitz, A.J. Heeger, F. Wudl, Photoinduced Electron Transfer from a Conducting Polymer to Buckminsterfullerene, *Science*. 258 (1992) 1474–1476. <https://doi.org/10.1126/science.258.5087.1474>.
- [3] G. Dennler, M.C. Scharber, C.J. Brabec, Polymer-Fullerene Bulk-Heterojunction Solar Cells, *Advanced Materials*. 21 (2009) 1323–1338. <https://doi.org/10.1002/adma.200801283>.

- [4] J. Nelson, Polymer:fullerene bulk heterojunction solar cells, *Materials Today*. 14 (2011) 462–470. [https://doi.org/10.1016/S1369-7021\(11\)70210-3](https://doi.org/10.1016/S1369-7021(11)70210-3).
- [5] G. Paternò, A. J. Warren, J. Spencer, G. Evans, V. García Sakai, J. Blumberger, F. Cacialli, Micro-focused X-ray diffraction characterization of high-quality [6,6]-phenyl-C 61 -butyric acid methyl ester single crystals without solvent impurities, *Journal of Materials Chemistry C*. 1 (2013) 5619–5623. <https://doi.org/10.1039/C3TC31075B>.
- [6] G. Paternò, F. Cacialli, V. García-Sakai, Structural and dynamical characterization of P3HT/PCBM blends, *Chemical Physics*. 427 (2013) 142–146. <https://doi.org/10.1016/j.chemphys.2013.10.006>.
- [7] G. Tregnago, M. Wykes, G.M. Paternò, D. Beljonne, F. Cacialli, Low-Temperature Photoluminescence Spectroscopy of Solvent-Free PCBM Single-Crystals, *J. Phys. Chem. C*. 119 (2015) 11846–11851. <https://doi.org/10.1021/acs.jpcc.5b02345>.
- [8] G.M. Lazzerini, G.M. Paternò, G. Tregnago, N. Treat, N. Stingelin, A. Yacoot, F. Cacialli, Traceable atomic force microscopy of high-quality solvent-free crystals of [6,6]-phenyl-C61-butyrac acid methyl ester, *Appl. Phys. Lett.* 108 (2016) 053303. <https://doi.org/10.1063/1.4941227>.
- [9] G.M. Paternò, M.W.A. Skoda, R. Dalgliesh, F. Cacialli, V.G. Sakai, Tuning Fullerene Intercalation in a Poly (thiophene) derivative by Controlling the Polymer Degree of Self-Organisation, *Scientific Reports*. 6 (2016) 34609. <https://doi.org/10.1038/srep34609>.
- [10] H.K.H. Lee, A.M. Telford, J.A. Röhr, M.F. Wyatt, B. Rice, J. Wu, A. de C. Maciel, S.M. Tuladhar, E. Speller, J. McGettrick, J.R. Searle, S. Pont, T. Watson, T. Kirchartz, J.R. Durrant, W.C. Tsoi, J. Nelson, Z. Li, The role of fullerenes in the environmental stability of polymer:fullerene solar cells, *Energy Environ. Sci*. 11 (2018) 417–428. <https://doi.org/10.1039/C7EE02983G>.
- [11] A. Wadsworth, M. Moser, A. Marks, M.S. Little, N. Gasparini, C.J. Brabec, D. Baran, I. McCulloch, Critical review of the molecular design progress in non-fullerene electron acceptors towards commercially viable organic solar cells, *Chem. Soc. Rev.* 48 (2019) 1596–1625. <https://doi.org/10.1039/C7CS00892A>.
- [12] R.S. Gurney, D.G. Lidzey, T. Wang, A review of non-fullerene polymer solar cells: from device physics to morphology control, *Rep. Prog. Phys.* 82 (2019) 036601. <https://doi.org/10.1088/1361-6633/ab0530>.
- [13] L. Duan, N.K. Elumalai, Y. Zhang, A. Uddin, Progress in non-fullerene acceptor based organic solar cells, *Solar Energy Materials and Solar Cells*. 193 (2019) 22–65. <https://doi.org/10.1016/j.solmat.2018.12.033>.
- [14] B. Fan, D. Zhang, M. Li, W. Zhong, Z. Zeng, L. Ying, F. Huang, Y. Cao, Achieving over 16% efficiency for single-junction organic solar cells, *Sci. China Chem.* 62 (2019) 746–752. <https://doi.org/10.1007/s11426-019-9457-5>.
- [15] J. Yuan, Y. Zhang, L. Zhou, G. Zhang, H.-L. Yip, T.-K. Lau, X. Lu, C. Zhu, H. Peng, P.A. Johnson, M. Leclerc, Y. Cao, J. Ulanski, Y. Li, Y. Zou, Single-Junction Organic Solar Cell with over 15% Efficiency Using Fused-Ring Acceptor with Electron-Deficient Core, *Joule*. 3 (2019) 1140–1151. <https://doi.org/10.1016/j.joule.2019.01.004>.
- [16] T. Yan, W. Song, J. Huang, R. Peng, L. Huang, Z. Ge, 16.67% Rigid and 14.06% Flexible Organic Solar Cells Enabled by Ternary Heterojunction Strategy, *Advanced Materials*. 31 (2019) 1902210. <https://doi.org/10.1002/adma.201902210>.
- [17] E. Kymakis, G.A.J. Amaratunga, CARBON NANOTUBES AS ELECTRON ACCEPTORS IN POLYMERIC PHOTOVOLTAICS, (n.d.) 6.
- [18] A.J. Ferguson, J.L. Blackburn, N. Kopidakis, Fullerenes and carbon nanotubes as acceptor materials in organic photovoltaics, *Materials Letters*. 90 (2013) 115–125. <https://doi.org/10.1016/j.matlet.2012.08.145>.

- [19] G. Soavi, F. Scotognella, D. Viola, T. Hefner, T. Hertel, G. Cerullo, G. Lanzani, High energetic excitons in carbon nanotubes directly probe charge-carriers, *Sci Rep.* 5 (2015) 1–5. <https://doi.org/10.1038/srep09681>.
- [20] M.D. Hanwell, D.E. Curtis, D.C. Lonie, T. Vandermeersch, E. Zurek, G.R. Hutchison, Avogadro: an advanced semantic chemical editor, visualization, and analysis platform, *Journal of Cheminformatics.* 4 (2012) 17. <https://doi.org/10.1186/1758-2946-4-17>.
- [21] F. Neese, The ORCA program system, *Wiley Interdisciplinary Reviews: Computational Molecular Science.* 2 (2012) 73–78. <https://doi.org/10.1002/wcms.81>.
- [22] C. Lee, W. Yang, R.G. Parr, Development of the Colle-Salvetti correlation-energy formula into a functional of the electron density, *Physical Review B.* 37 (1988) 785–789. <https://doi.org/10.1103/PhysRevB.37.785>.
- [23] A. Schäfer, H. Horn, R. Ahlrichs, Fully optimized contracted Gaussian basis sets for atoms Li to Kr, *The Journal of Chemical Physics.* 97 (1992) 2571–2577. <https://doi.org/10.1063/1.463096>.
- [24] A. Schäfer, C. Huber, R. Ahlrichs, Fully optimized contracted Gaussian basis sets of triple zeta valence quality for atoms Li to Kr, *The Journal of Chemical Physics.* 100 (1994) 5829–5835. <https://doi.org/10.1063/1.467146>.
- [25] K. Eichkorn, F. Weigend, O. Treutler, R. Ahlrichs, Auxiliary basis sets for main row atoms and transition metals and their use to approximate Coulomb potentials, *Theoretical Chemistry Accounts: Theory, Computation, and Modeling (Theoretica Chimica Acta).* 97 (1997) 119–124. <https://doi.org/10.1007/s002140050244>.
- [26] E.~F.~Valeev, A library for the evaluation of molecular integrals of many-body operators over Gaussian functions, (2014). <http://libint.valeyev.net/>.
- [27] S. Lehtola, C. Steigemann, M.J.T. Oliveira, M.A.L. Marques, Recent developments in libxc — A comprehensive library of functionals for density functional theory, *SoftwareX.* 7 (2018) 1–5. <https://doi.org/10.1016/j.softx.2017.11.002>.
- [28] M.A.L. Marques, M.J.T. Oliveira, T. Burnus, Libxc: A library of exchange and correlation functionals for density functional theory, *Computer Physics Communications.* 183 (2012) 2272–2281. <https://doi.org/10.1016/j.cpc.2012.05.007>.
- [29] F. Weigend, R. Ahlrichs, Balanced basis sets of split valence, triple zeta valence and quadruple zeta valence quality for H to Rn: Design and assessment of accuracy, *Phys. Chem. Chem. Phys.* 7 (2005) 3297–3305. <https://doi.org/10.1039/B508541A>.
- [30] F. Weigend, Accurate Coulomb-fitting basis sets for H to Rn, *Phys. Chem. Chem. Phys.* 8 (2006) 1057–1065. <https://doi.org/10.1039/B515623H>.
- [31] Y. Carissan, D. Hagebaum-Reignier, N. Goudard, S. Humbel, Hückel-Lewis Projection Method: A “Weights Watcher” for Mesomeric Structures, *J. Phys. Chem. A.* 112 (2008) 13256–13262. <https://doi.org/10.1021/jp803813e>.
- [32] Huckel Theory and HuLiS: a calculator that also describes mesomerism., (2013). <http://www.hulis.free.fr/> (accessed June 8, 2020).
- [33] Y. Kim, C.E. Song, S.-J. Moon, E. Lim, Effect of dye end groups in non-fullerene fluorene- and carbazole-based small molecule acceptors on photovoltaic performance, *RSC Adv.* 5 (2015) 62739–62746. <https://doi.org/10.1039/C5RA03607K>.
- [34] Y. Kim, C.E. Song, S.-J. Moon, E. Lim, Rhodanine dye-based small molecule acceptors for organic photovoltaic cells, *Chem. Commun.* 50 (2014) 8235–8238. <https://doi.org/10.1039/C4CC01695E>.
- [35] A.D. Hendsbee, J.-P. Sun, W.K. Law, H. Yan, I.G. Hill, D.M. Spasyuk, G.C. Welch, Synthesis, Self-Assembly, and Solar Cell Performance of N-Annulated Perylene Diimide Non-Fullerene Acceptors, *Chem. Mater.* 28 (2016) 7098–7109. <https://doi.org/10.1021/acs.chemmater.6b03292>.

- [36] S. Li, L. Ye, W. Zhao, S. Zhang, S. Mukherjee, H. Ade, J. Hou, Energy-Level Modulation of Small-Molecule Electron Acceptors to Achieve over 12% Efficiency in Polymer Solar Cells, *Advanced Materials*. 28 (2016) 9423–9429. <https://doi.org/10.1002/adma.201602776>.
- [37] W. Zhao, S. Li, H. Yao, S. Zhang, Y. Zhang, B. Yang, J. Hou, Molecular Optimization Enables over 13% Efficiency in Organic Solar Cells, *J. Am. Chem. Soc.* 139 (2017) 7148–7151. <https://doi.org/10.1021/jacs.7b02677>.

Supporting Information

Cz-RH

ABSORPTION SPECTRUM VIA TRANSITION ELECTRIC DIPOLE MOMENTS

State	Energy (cm-1)	Wavelength (nm)	fosc	T2 (au**2)	TX (au)	TY (au)	TZ (au)
1	20425.0	489.6	2.636921809	42.50219	-6.50477	-0.06649	0.43090
2	21881.8	457.0	0.000280760	0.00422	0.05491	-0.02345	0.02567
3	21884.8	456.9	0.000668999	0.01006	-0.09583	-0.01729	0.02410
4	22144.9	451.6	0.003095696	0.04602	0.01806	0.20002	-0.07540
5	24264.7	412.1	0.006812285	0.09243	0.00579	-0.30385	-0.00816
6	25467.6	392.7	0.918517216	11.87340	-3.43772	-0.05104	0.23001
7	25912.9	385.9	0.117947044	1.49847	0.14975	1.21270	-0.07351
8	25956.8	385.3	0.250613803	3.17855	-1.77458	0.13092	0.11076
9	27101.0	369.0	0.000023860	0.00029	-0.00361	0.01631	0.00330
10	27106.8	368.9	0.000033068	0.00040	-0.00495	0.01900	0.00400
11	27614.2	362.1	0.151963043	1.81168	1.34274	0.01873	-0.09157
12	29882.5	334.6	0.054487583	0.60028	0.00407	-0.75792	-0.16071
13	30997.0	322.6	0.026028282	0.27644	-0.52413	-0.00848	0.04072
14	31166.8	320.9	0.001844360	0.01948	0.00753	0.04215	0.13285
15	31499.9	317.5	0.000115857	0.00121	-0.03455	-0.00404	0.00079
16	31514.8	317.3	0.000127357	0.00133	0.03622	-0.00223	-0.00371

Flu-RH

ABSORPTION SPECTRUM VIA TRANSITION ELECTRIC DIPOLE MOMENTS

State	Energy (cm-1)	Wavelength (nm)	fosc	T2 (au**2)	TX (au)	TY (au)	TZ (au)
1	20238.5	494.1	2.748812476	44.71379	6.67292	0.05268	-0.42800
2	21796.2	458.8	0.000098328	0.00149	0.00273	0.02174	-0.03170
3	21797.2	458.8	0.000540438	0.00816	0.08993	0.00395	-0.00769
4	22013.1	454.3	0.000930133	0.01391	0.00428	0.10743	-0.04849
5	25578.7	391.0	1.073938741	13.82219	3.70979	0.06625	-0.23501
6	25785.8	387.8	0.081275472	1.03766	-0.15148	1.00541	0.06220
7	26944.6	371.1	0.000040679	0.00050	-0.01780	0.01176	0.00648
8	26958.9	370.9	0.000027984	0.00034	0.01013	-0.01400	-0.00656
9	27443.0	364.4	0.143069407	1.71629	-1.30724	-0.01550	0.08467
10	29786.5	335.7	0.046371071	0.51251	0.00493	0.68594	0.20488
11	30940.8	323.2	0.015361888	0.16345	-0.40366	0.00033	0.02257
12	31038.0	322.2	0.005879600	0.06236	-0.00783	-0.20036	-0.14886
13	31359.3	318.9	0.000051734	0.00054	-0.02286	0.00447	0.00083
14	31368.8	318.8	0.000115066	0.00121	-0.03317	-0.01019	-0.00188
15	31484.3	317.6	0.000575788	0.00602	0.00268	0.04150	0.06551
16	31890.3	313.6	0.000009507	0.00010	0.00927	0.00098	-0.00334

TPDI-Hex

DFT B3LYP

ABSORPTION SPECTRUM VIA TRANSITION ELECTRIC DIPOLE MOMENTS

State	Energy (cm-1)	Wavelength (nm)	fosc	T2 (au**2)	TX (au)	TY (au)	TZ (au)
1	18633.1	536.7	0.001188915	0.02101	0.07273	-0.03149	0.12135
2	18666.3	535.7	0.002281881	0.04024	0.16884	-0.08138	0.07151
3	22147.5	451.5	0.806393685	11.98665	-1.99709	-2.82305	-0.16935

4	22367.8	447.1	0.694764420	10.22564	1.46986	-0.89662	-2.69466
5	24227.7	412.8	0.015520783	0.21090	-0.11319	-0.36717	0.25155
6	24257.6	412.2	0.015732386	0.21351	-0.06679	0.45708	0.01135
7	24436.0	409.2	0.251680624	3.39075	1.10583	-1.10701	0.97079
8	24754.8	404.0	0.012369662	0.16450	0.18705	-0.09861	-0.34611
9	26248.4	381.0	0.000181507	0.00228	0.00524	0.03785	0.02858
10	26264.2	380.7	0.000180823	0.00227	0.03578	0.01645	-0.02675
11	26549.3	376.7	0.000097562	0.00121	0.01797	-0.00552	-0.02926
12	26550.5	376.6	0.000183039	0.00227	0.02252	0.04186	0.00320
13	29092.8	343.7	0.039767148	0.45000	-0.38904	0.11121	0.53506
14	29099.1	343.7	0.040884198	0.46254	0.45870	0.45191	0.21888
15	29526.7	338.7	0.019212493	0.21421	-0.03458	0.34812	-0.30303
16	29540.0	338.5	0.032098441	0.35773	0.19759	-0.55445	0.10613

ZINDO/S

ABSORPTION SPECTRUM VIA TRANSITION ELECTRIC DIPOLE MOMENTS

State	Energy (cm-1)	Wavelength (nm)	fosc	T2 (au**2)	TX (au)	TY (au)	TZ (au)
1	20353.5	491.3	0.929551124	15.03524	2.17953	3.20322	0.15590
2	20566.8	486.2	0.824032123	13.19025	-1.68079	1.00422	3.05888
3	24606.3	406.4	0.370722871	4.95997	-1.28858	1.39716	-1.16081
4	24829.9	402.7	0.006722335	0.08913	-0.12538	0.05557	0.26518
5	26308.3	380.1	0.000300105	0.00376	-0.00872	0.05801	-0.01772
6	26312.2	380.1	0.000141289	0.00177	-0.01658	-0.00055	0.03864
7	28382.8	352.3	0.001088332	0.01262	0.08222	0.07276	0.02387
8	28425.6	351.8	0.000536435	0.00621	-0.03864	0.02199	0.06509
9	28883.2	346.2	0.017044440	0.19427	0.34113	-0.15029	0.23519
10	28919.3	345.8	0.000728793	0.00830	-0.02610	0.01597	0.08579
11	29147.3	343.1	0.085091643	0.96109	-0.68880	0.45148	-0.53180
12	29553.0	338.4	0.001389122	0.01547	0.05864	-0.03093	-0.10525
13	30740.3	325.3	0.001205058	0.01291	-0.00910	0.07221	0.08722
14	30743.1	325.3	0.001194424	0.01279	0.08712	0.05875	-0.04182
15	30873.6	323.9	0.000641028	0.00684	0.00639	0.05821	0.05836
16	30874.6	323.9	0.000634851	0.00677	0.06310	0.02686	-0.04545

ITIC-4F

DFT B3LYP

ABSORPTION SPECTRUM VIA TRANSITION ELECTRIC DIPOLE MOMENTS

State	Energy (cm-1)	Wavelength (nm)	fosc	T2 (au**2)	TX (au)	TY (au)	TZ (au)
1	16021.3	624.2	3.151945843	64.76723	-8.00573	0.81924	0.06586
2	18005.8	555.4	0.000078746	0.00144	-0.00239	-0.00050	-0.03787
3	20505.4	487.7	0.369288338	5.92887	-2.33422	0.69293	0.01248
4	20718.9	482.7	0.000018914	0.00030	-0.00336	0.00127	0.01696
5	22754.0	439.5	0.000040494	0.00059	0.00134	-0.00132	-0.02413
6	22847.2	437.7	0.217244089	3.13034	1.74375	-0.29914	-0.01355
7	23430.8	426.8	0.063449449	0.89149	-0.86504	-0.37819	0.01301
8	23683.6	422.2	0.322638641	4.48482	-2.11764	-0.00381	0.02019
9	23723.4	421.5	0.000127641	0.00177	-0.02349	0.00331	0.03477
10	24396.5	409.9	0.000517467	0.00698	-0.00151	-0.00026	-0.08355
11	24933.1	401.1	0.045630591	0.60250	-0.75371	0.18546	0.00547
12	25489.7	392.3	0.000001187	0.00002	0.00134	-0.00031	-0.00367
13	25745.6	388.4	0.001914986	0.02449	-0.12496	0.09419	-0.00059
14	25791.3	387.7	0.000225667	0.00288	0.00031	0.00177	0.05364

15	25927.0	385.7	0.000228345	0.00290	-0.00019	0.00048	0.05384
16	26014.3	384.4	0.000883690	0.01118	0.05332	0.09129	-0.00236

ZINDO/S

 ABSORPTION SPECTRUM VIA TRANSITION ELECTRIC DIPOLE MOMENTS

State	Energy (cm-1)	Wavelength (nm)	fosc	T2 (au**2)	TX (au)	TY (au)	TZ (au)
1	14667.1	681.8	2.059597359	46.22895	6.76043	-0.72285	-0.05526
2	17736.9	563.8	0.000251870	0.00467	-0.00038	-0.00154	-0.06836
3	22654.8	441.4	0.092704389	1.34715	-0.31402	-1.11721	0.01945
4	22761.7	439.3	0.000011792	0.00017	-0.00030	-0.00092	0.01302
5	25033.4	399.5	0.004722716	0.06211	-0.21593	0.12443	0.00069
6	25037.1	399.4	0.000052211	0.00069	-0.02218	0.01275	0.00566
7	25073.7	398.8	0.047222160	0.62002	-0.68500	0.38830	0.00282
8	26636.3	375.4	0.000193395	0.00239	0.00054	0.00077	0.04888
9	28070.7	356.2	0.004324019	0.05071	-0.00170	-0.00283	-0.22517
10	28173.3	354.9	0.005101163	0.05961	-0.05964	-0.23673	0.00293
11	29017.7	344.6	0.129519437	1.46943	-0.36003	1.15743	-0.01290
12	30150.3	331.7	0.527586376	5.76073	-0.49875	-2.34744	0.03893
13	30356.6	329.4	0.002217881	0.02405	0.00205	0.00364	0.15503
14	30995.4	322.6	0.001535878	0.01631	-0.00075	-0.00516	-0.12762
15	31347.0	319.0	0.041230077	0.43301	-0.09580	0.65098	-0.00708
16	31662.5	315.8	0.000041130	0.00043	-0.00086	-0.00085	-0.02064

BTPTT-4F

DFT B3LYP

 ABSORPTION SPECTRUM VIA TRANSITION ELECTRIC DIPOLE MOMENTS

State	Energy (cm-1)	Wavelength (nm)	fosc	T2 (au**2)	TX (au)	TY (au)	TZ (au)
1	16047.9	623.1	2.847576407	58.41607	7.63172	0.41363	-0.04208
2	18175.9	550.2	0.118290371	2.14254	-0.09690	1.45952	-0.05447
3	20765.2	481.6	0.406771754	6.44898	-2.53572	-0.13792	0.00920
4	21119.6	473.5	0.047485016	0.74020	-0.04818	0.85786	-0.04422
5	21257.5	470.4	0.002358955	0.03653	0.01275	-0.19009	0.01532
6	22445.5	445.5	0.080785539	1.18490	1.08686	0.06001	-0.00607
7	23185.9	431.3	0.147507340	2.09442	-1.44469	-0.08472	0.01019
8	23403.9	427.3	0.007233836	0.10175	-0.31872	-0.01283	0.00305
9	23991.1	416.8	0.525483349	7.21083	0.13973	-2.68005	0.09282
10	24261.7	412.2	0.102003309	1.38410	1.17568	0.04285	-0.00653
11	24834.9	402.7	0.151573874	2.00926	0.08111	-1.41427	0.05031
12	25215.4	396.6	0.000805821	0.01052	0.01092	0.10165	0.00823
13	25245.7	396.1	0.000061430	0.00080	0.00551	-0.02589	-0.01003
14	26209.2	381.5	0.004901461	0.06157	-0.01504	0.24705	-0.01752
15	26493.3	377.5	0.012859732	0.15980	0.39871	0.02648	-0.01127
16	27232.3	367.2	0.017631933	0.21315	0.01928	-0.46086	0.01965

ZINDO/S

 ABSORPTION SPECTRUM VIA TRANSITION ELECTRIC DIPOLE MOMENTS

State	Energy (cm-1)	Wavelength (nm)	fosc	T2 (au**2)	TX (au)	TY (au)	TZ (au)
1	13773.9	726.0	1.746736906	41.74901	6.45188	0.34797	-0.03449
2	18337.0	545.3	0.413742478	7.42808	-0.14737	2.71997	-0.09002

3	20266.6	493.4	0.122671336	1.99268	-1.40960	-0.07498	0.01004
4	23979.0	417.0	0.044038567	0.60461	0.77742	0.01025	0.01096
5	24006.2	416.6	0.063920902	0.87659	0.02485	-0.93318	0.07177
6	25109.7	398.3	0.036403897	0.47729	0.03797	-0.68923	0.02837
7	25446.5	393.0	0.000007672	0.00010	0.00255	-0.00322	-0.00908
8	25452.7	392.9	0.000018754	0.00024	-0.01057	-0.00711	-0.00896
9	27131.1	368.6	0.003406432	0.04133	0.20284	0.01141	0.00761
10	28539.6	350.4	0.150764843	1.73911	0.07150	-1.31384	0.08848
11	29272.4	341.6	0.191892753	2.15812	-1.46677	-0.08173	-0.00556
12	29721.5	336.5	0.010096900	0.11184	-0.01540	0.33164	-0.04019
13	30233.1	330.8	0.314421493	3.42378	1.84614	0.12341	0.01772
14	30421.1	328.7	0.495462123	5.36181	-0.14231	2.30408	-0.18103
15	31211.5	320.4	0.030617713	0.32295	-0.03281	0.56559	-0.04448
16	31768.1	314.8	0.004289706	0.04445	0.21045	0.01278	-0.00103